New Journal of Physics
The open access journal at the forefront of physics

Deutsche Physikalische Gesellschaft DPG IOP Institute of Physics

Entangling microscopic defects via a macroscopic quantum shuttle

To cite this article: G J Grabovskij *et al* 2011 *New J. Phys.* **13** 063015

New Journal of Physics
The open-access journal for physics

Entangling microscopic defects via a macroscopic quantum shuttle

G J Grabovskij[1], P Bushev[1], J H Cole[2,3], C Müller[3,4], J Lisenfeld[1], A Lukashenko[1] and A V Ustinov[1,3,5]

[1] Physikalisches Institut, Karlsruhe Institute of Technology, D-76128 Karlsruhe, Germany
[2] Institut für Theoretische Festkörperphysik, Karlsruhe Institute of Technology, D-76128 Karlsruhe, Germany
[3] DFG-Center for Functional Nanostructures (CFN), D-76128 Karlsruhe, Germany
[4] Institut für Theorie der Kondensierten Materie, Karlsruhe Institute of Technology, D-76128 Karlsruhe, Germany
E-mail: ustinov@kit.edu

New Journal of Physics **13** (2011) 063015 (10pp)
Received 21 February 2011
Published 9 June 2011
Online at http://www.njp.org/
doi:10.1088/1367-2630/13/6/063015

Abstract. In the microscopic world, multipartite entanglement has been achieved with various types of nanometer-sized two-level systems such as trapped ions, atoms and photons. On the macroscopic scale ranging from micrometers to millimeters, recent experiments have demonstrated bipartite and tripartite entanglement for electronic quantum circuits with superconducting Josephson junctions. It remains challenging to bridge these largely different length scales by constructing hybrid quantum systems. Doing so may allow us to manipulate the entanglement of individual microscopic objects separated by macroscopically large distances in a quantum circuit. Here we report on the experimental demonstration of induced coherent interaction between two intrinsic two-level states (TLSs) formed by atomic-scale defects in a solid via a superconducting phase qubit. The tunable superconducting circuit serves as a shuttle communicating quantum information between the two microscopic TLSs. We present a detailed comparison between experiment and theory and find excellent agreement over a wide range of parameters. We then use the theoretical model to study the creation and movement of entanglement between the three components of the quantum system.

[5] Author to whom any correspondence should be addressed.

Contents

1. Introduction

Controllable coherent interaction between individual quantum systems is one of the fundamental prerequisites for quantum information processing. This interaction allows one to selectively entangle systems and to transfer quantum information between its individual parts. The demonstration of such tunable interaction, allowing each individual part of a system to controllably interact with every other part, is therefore a major step towards demonstrating the possible use of a particular architecture for quantum information processing [1]. In atomic systems, such quantum information transfer and processing are established, for example, via long-range Coulomb [2] or magnetic dipole interactions [3]. Photonic systems utilize the Kerr-type interaction in nonlinear crystals [4], whereas for superconducting qubits the interaction is defined by the circuit design [5, 6]. In order to achieve tunability, it has proved useful to introduce an additional quantum system acting as a mediator of the interaction between two parts. This role can be played, for example, by a resonant cavity or additional, so-called *ancilla* qubits [7, 8]. The use of ancilla qubits has been demonstrated, for example, with electron and nuclear spins of ^{13}C atoms in NV-defect centers of diamond [3] and with superconducting flux qubits [9]. For superconducting systems, the use of a microwave cavity placed on the same chip has proved very useful [10, 11]. For superconducting qubits, due to their nature as part of an electronic circuit, the effect of the environment on the dynamics is often very strong. This has led to a much better understanding of the nature of the environment, as well as to improved qubit designs that are insensitive to certain of its characteristics [12, 13]. One part of the environment is formed by the so-called two-level defect states (TLSs). Ensembles of these TLSs are a general model for decoherence [14, 15] in a wide variety of systems including glasses and mechanical resonators [16–21]. In superconducting phase qubits, which have large-area Josephson junctions, one often finds signatures of individual two-level systems resonantly interacting with the qubit [22]. TLSs are in general thought to be detrimental to the operation of the qubit [23, 24], but since they are often more coherent than the qubit and their potential use as a quantum memory has been demonstrated [25], it has been proposed to use the TLS itself as computational qubits [26].

In this paper, we demonstrate a coherent interaction between two microscopic defect states mediated by a superconducting phase qubit. The TLSs have fixed but different resonant frequencies, and the phase qubit works as a frequency-tunable shuttle communicating quantum information between them. The observed dynamical quantum beating signal between all three

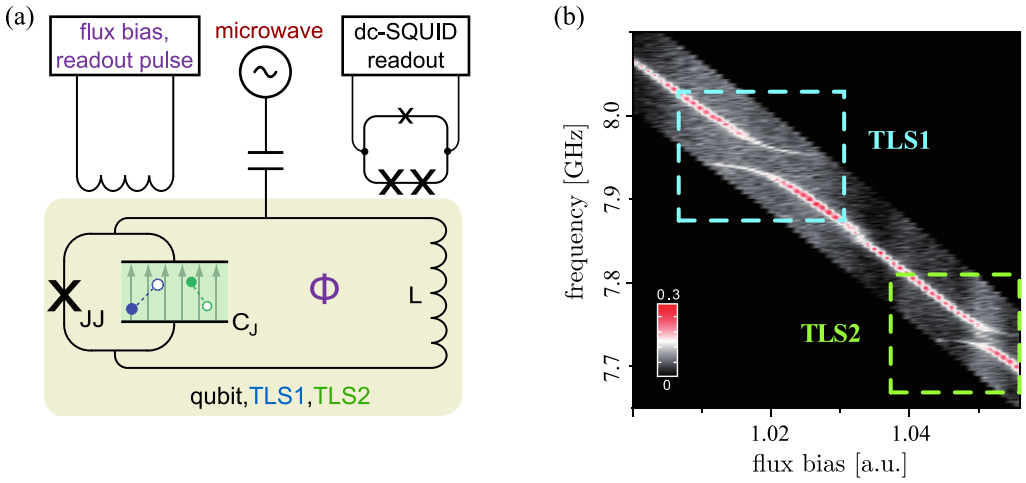

Figure 1. (a) Sketch of the experimental setup and circuit of the phase qubit with two TLSs residing inside the qubit's Josephson junction. (b) Excitation spectrum of the phase qubit showing two avoided level crossings due to the coupling with TLS1 and TLS2. The color bar denotes the excitation probability of the qubit.

Table 1. The characteristics of the three subsystems: qubit, TLS1 and TLS2. The resonance frequencies and the couplings between the qubit and the TLSs are denoted by ω and v, respectively. The range for the holding position of the qubit ω_h is 7.65–8.00 GHz, covering the resonance frequencies of the TLSs. The characteristic times are denoted by T_1 (relaxation time) and T_2 (dephasing time as measured using a Ramsey experiment).

	Qubit	TLS1	TLS2
$\omega/2\pi$ (GHz)	–	7.946	7.735
$v/2\pi$ (MHz)	–	36	23
T_1 (ns)	120	380	410
T_2 (ns)	90	580	810

systems verifies the multipartite interaction and the basic operations presented here offer the possibility of establishing coherent control over many TLSs coupled to the Josephson junction of any flux or phase qubit. A sketch of the experimental setup is shown in figure 1(a). The sample is maintained at a temperature of around 35 mK in a dilution refrigerator. For details of the experimental setup, see [27]. The coupling between the qubit and TLSs leads to characteristic anticrossings in qubit spectroscopy (figure 1(b)). From their positions and sizes, one can infer the level splitting of the TLSs as well as the strength of their coupling to the qubit. Using resonant microwave driving of the TLSs when the qubit is far detuned [28], we are able to determine their coherence properties. Table 1 gives eigenenergies ω, coupling strengths v and the relaxation and dephasing rates for the qubit and both TLSs. Note that the decoherence times of the TLSs are much longer in comparison to the phase qubit, and one of them shows T_1-limited dephasing [28].

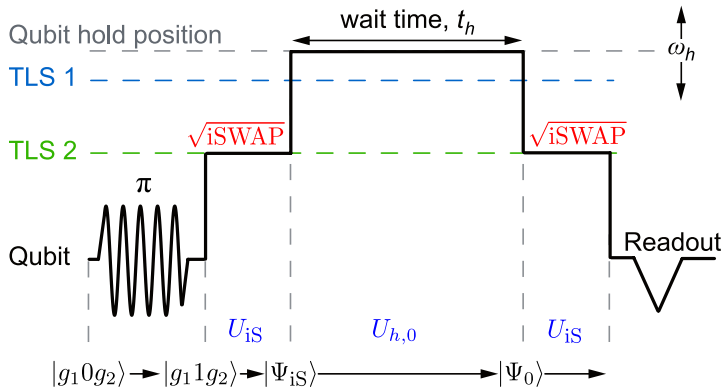

Figure 2. The experimental sequence used to establish a coherent interaction between a phase qubit and a pair of TLSs. The qubit is first excited using a π-pulse. The frequency of the qubit is then tuned to be resonant with TLS2 in order to realize an $\sqrt{\text{iSWAP}}$-gate. The qubit is then biased at some frequency ω_{h} lying in the range that covers the resonances of both TLSs and is held there for some time t_{h}. A subsequent $\sqrt{\text{iSWAP}}$ with TLS2 and readout then gives a direct signal of the interaction between the TLSs induced by the qubit.

2. Establishing a coherent interaction between the three subsystems

The pulse sequence applied to the circuit is shown in figure 2. Initially, the entire system is prepared in its ground state. The qubit is detuned away from both TLSs and excited with a π-pulse. A fast flux bias pulse (of rise time 2 ns) brings it in resonance with TLS2 and keeps it there for a fixed time to perform an $\sqrt{\text{iSWAP}}$-gate [25, 29]. After this gate, one half of the excitation remains in the qubit and the other half is transferred to TLS2, resulting in an entangled state between these subsystems. To induce an interaction between all three components of our system, the qubit is then tuned to a frequency ω_{h} and is held there for a time t_{h}. This hold position (ω_{h}) is varied over a range that includes the resonance frequencies of both TLSs. Depending on the detuning between qubit and TLS1 or TLS2 (Δ_{q1}, Δ_{q2}) and the hold time, the qubit acquires a phase with respect to TLS2 as well as exchanging population with one or both TLSs. The population and acquired phase of the qubit can be revealed by performing an additional $\sqrt{\text{iSWAP}}$-gate between the qubit and TLS2 followed by a readout of the qubit. The results can be compared with an interference pattern. Depending on the relative phase between the qubit and TLS2 the interference can be constructive or destructive, resulting in energy being transferred to the qubit or to TLS2. The advantage of the protocol used here, in comparison to, for example, just measuring the beating between the qubit and a TLS as a function of detuning, is that the visibility does not decrease with detuning but depends only on the phase difference between the qubit and TLS2 (and the dephasing processes).

3. Analysis of the experimental results

The measured escape probability, which corresponds to the probability of measuring the qubit in its excited state, is presented in figure 3(a). The experiment was carried out in two ranges such that the qubit is held close to the resonance with either TLS, resulting in two chevron patterns.

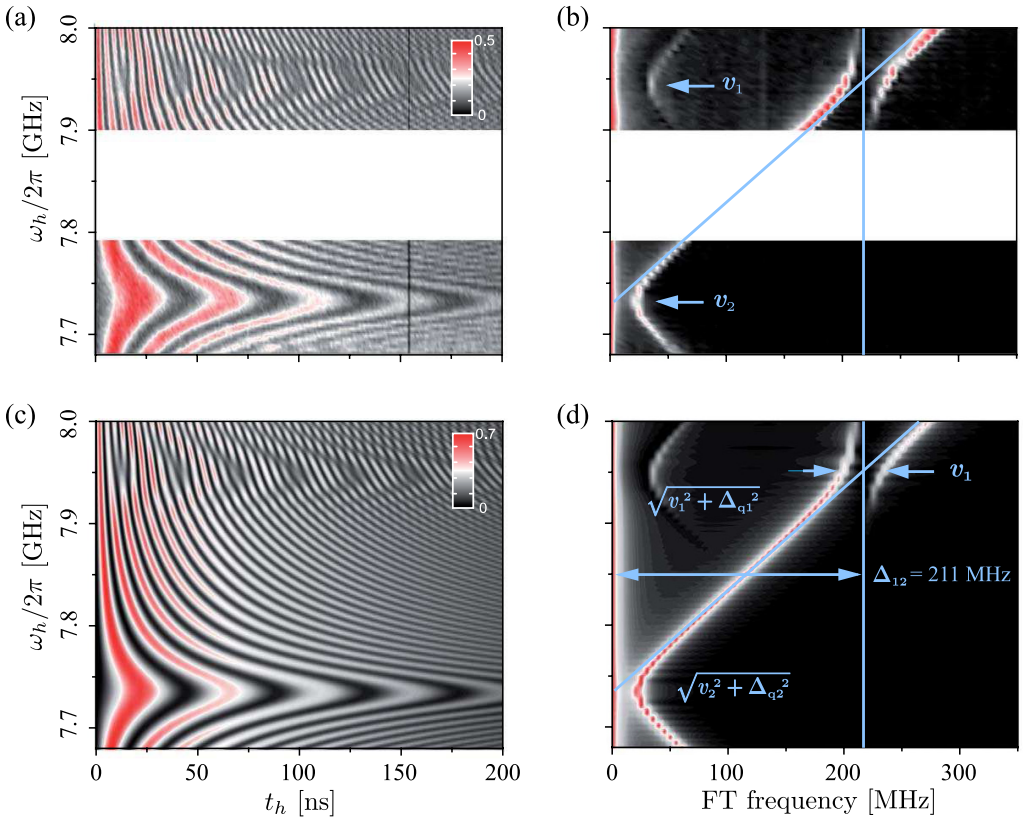

Figure 3. Time and frequency domain evolution of the combined qubit–TLS1–TLS2 system. Experimental (a) and theoretical (c) beating signals of the qubit state with two TLSs. The color bar shows the measured/calculated escape probability for the phase qubit. Experimental (b) and theoretical (d) FT of the beating signal showing hyperbolas due to interaction between the qubit and each of the TLSs. The vertical blue line indicates the TLS1–TLS2 detuning Δ_{21}. The diagonal blue line follows the relation $\omega_2 + \Delta_{q2}$. The anticrossing on TLS2 hyperbola appears in resonance with TLS1 at a frequency of Δ_{12} and indicates the established interaction between two defects via the phase qubit.

Figure 3(c) shows the result of a numerical simulation, which corresponds well to the measured results. The time dependence of the system is calculated via the evolution of the density matrix of the whole system [30] including decoherence in the Lindblad form [31]. The parameters for the simulation are taken from independent measurements of the various coupling parameters and decoherence rates (cf table 1). To study the system dynamics in greater detail, we solve the coherent evolution of the system analytically at key points of interest. The resulting expressions for the escape probability (see below) display the same qualitative behavior as the full numerical simulations shown in figures 3(c) and (d) and figure 4.

The lower chevron in figures 3(a) and (c) corresponds to the situation when the qubit is held close to TLS2 and the observed oscillations simply correspond to energy transfer between the qubit and TLS2. If we neglect the coupling to TLS1, the probability of finding the qubit in

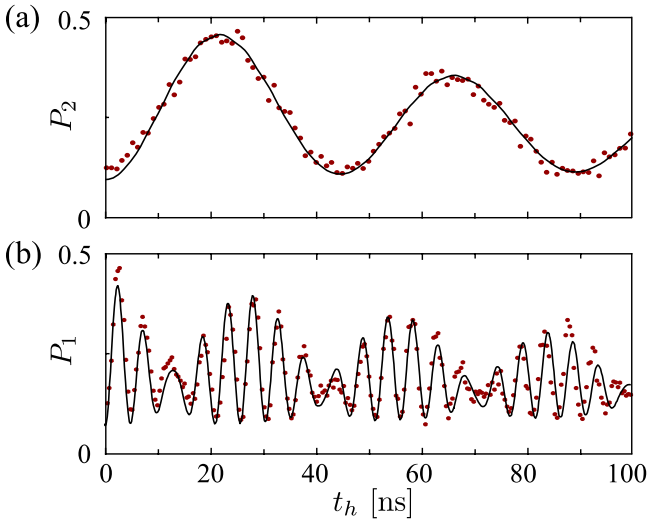

Figure 4. Dynamics of the final qubit population at each of the TLS resonances. The simulated (solid line) and measured (dots) qubit occupation probabilities at the holding position of the qubit ω_h in resonance with TLS2 (a) and TLS1 (b).

its excited state while exactly in resonance with TLS2 can be expressed as

$$P_2(t_h) \approx \tfrac{1}{2}\,(1 - \cos v_2 t_h). \tag{1}$$

This shows the simple oscillations with frequency of the qubit–TLS coupling that enables one to coherently transfer information between the qubit and TLS. The comparison between the theory and experiment for this case is shown in figure 4(a) at the point $\omega_h = \omega_2$. Both curves are extracted from the plots in figures 3(a) and (c). The probability of the theoretical curve is scaled linearly to match the observed measurement visibility.

As mentioned above, the protocol used here allows us to detune the qubit far from the resonance with TLS2 without loss of visibility. This can be seen from figure 3(a), where a clear oscillatory signal is observed over the range of more than 300 MHz. The equivalent theoretical plot can be seen in figure 3(c). In the vicinity of TLS1, the chevron pattern develops an additional overlaid feature, which is similar in structure to TLS2. It is exactly this feature that is the signature of the induced TLS–TLS coupling. At the point where the qubit is held resonant with TLS1, we can obtain a simplified analytical expression for the measurement probability by assuming that the qubit is decoupled from one TLS while being in resonance with the other (the derivation of equations (1) and (2) will be discussed in detail later):

$$P_1(t_h) \approx \left(\frac{3}{8} + \frac{1}{8}\cos v_1 t_h - \frac{1}{2}\cos\frac{v_1 t_h}{2}\cos\Delta_{21} t_h\right), \tag{2}$$

where $\Delta_{21} = 2\pi \times 211$ MHz is the frequency difference between the two TLSs. This expression shows temporal beating of the qubit population due to the induced coherent interaction with the three frequencies v_1, $\Delta_{21} - v_1/2$ and $\Delta_{21} + v_1/2$. The experimental and theoretical curves at $\omega_h = \omega_1$ are extracted from figures 3(a) and (c) and plotted in figure 4(b) (the theoretical curve is again scaled linearly to match the experiment).

To see the three frequency components more clearly, we show the Fourier transform (FT) of the measured (figure 3(b)), and simulated (figure 3(d)), temporal evolutions of the

escape probability. The frequency spectra contain the hyperbola $\sqrt{v_2^2 + \Delta_{q2}^2}$ that relates the swap frequency with the qubit–TLS2 detuning Δ_{q2}. This hyperbola shows an anticrossing in the vicinity of TLS1, which has a splitting size equal to $v_1 = 36\,\mathrm{MHz}$ at the detuning frequency of $\Delta_{21} = 211\,\mathrm{MHz}$. Furthermore, an additional hyperbola $\sqrt{v_1^2 + \Delta_{q1}^2}$ appears due to the direct coupling between the qubit and TLS1. Here we stress that the fact that the *three fundamental frequencies* appear in the system's dynamic indicates the established interaction between all three parts of the system and cannot be attributed to the interaction between any two parts.

4. Theoretical description

In addition to the numerical simulation of the three coupled two-level quantum systems including decoherence effects [30], we also present a simplified theoretical picture yielding the two analytical expressions (1) and (2). The Hamiltonian H of the entire system depends on the frequency of the qubit, ω_q, and of the TLSs, ω_i, $i = 1, 2$, and on the interaction parts between the qubit and the TLSs, v_i, $i = 1, 2$:

$$H_0(\omega_q) = \frac{\hbar}{2}[\omega_q\sigma_z + \omega_1\tau_{1,z} + \omega_2\tau_{2,z} + v_1(\sigma_-\tau_{1,+} + \sigma_+\tau_{1,-}) + v_2(\sigma_-\tau_{2,+} + \sigma_+\tau_{2,-})], \tag{3}$$

with σ and τ_i, $i = 1, 2$, being the Pauli matrices for the qubit and TLSs, respectively. In the following, $|0\rangle$, $|1\rangle$ will denote the states of the qubit and $|g_i\rangle$, $|e_i\rangle$, $i = 1, 2$, that of TLS1 and TLS2, respectively. The exact solution of the time evolution of the system, although tractable, is too complicated to provide useful insights. A clearer understanding is obtained by solving the time evolution without decoherence in the limit that the qubit in the vicinity of one TLS is decoupled from the other TLS. This approximation is justified in the case when $\Delta_{21} \gg v_1, v_2$. In this limit, the Hamiltonian becomes

$$H_i = H_0(\omega_q = \omega_i) \approx \frac{\hbar}{2}[\omega_i\sigma_z + \omega_1\tau_{1,z} + \omega_2\tau_{2,z} + v_i(\sigma_-\tau_{i,+} + \sigma_+\tau_{i,-})], \tag{4}$$

where $i = 1, 2$ indicates resonance with TLS1 or TLS2, respectively. We are still able to describe the beating due to the effect of the two TLSs as the qubit is brought into resonance with each in turn. The operator $U_{\mathrm{iS}} = \exp(-\mathrm{i}H_2 t_{\mathrm{iS}}/\hbar)$ describes the $\sqrt{\mathrm{iSWAP}}$-gate operation between the qubit and TLS2 while neglecting the interaction with TLS1. Here $t_{\mathrm{iS}} = \pi/(2v_2)$ is the time needed for the gate. The evolution of the state vector during the holding time is given by the unitary operator $U_{\mathrm{h},0}(\omega_{\mathrm{h}}, t_{\mathrm{h}}) = \exp(-\mathrm{i}H_0(\omega_{\mathrm{h}})t_{\mathrm{h}}/\hbar)$, which under our approximation gives us the approximate operators $U_{\mathrm{h},i}(t_{\mathrm{h}}) = \exp(-\mathrm{i}H_i t_{\mathrm{h}}/\hbar)$, $i = 1, 2$.

Starting with the ground state $|g_1 0 g_2\rangle$, the qubit is excited, which results in the state $|g_1 1 g_2\rangle$. The state after the first $\sqrt{\mathrm{iSWAP}}$ is then given by $|\Psi_{\mathrm{iS}}\rangle = U_{\mathrm{iS}}|g_1 1 g_2\rangle = (|g_1 1 g_2\rangle - \mathrm{i}|g_1 0 e_2\rangle)/\sqrt{2}$. In the next step, the interaction between all components of our system is established. Including the full Hamiltonian in the time evolution, this is described by the equation $|\Psi_0(\omega_{\mathrm{h}}, t_{\mathrm{h}})\rangle = U_{\mathrm{h},0}(\omega_{\mathrm{h}}, t_{\mathrm{h}})U_{\mathrm{iS}}|g_1 1 g_2\rangle$. Finally, after performing the second $\sqrt{\mathrm{iSWAP}}$-gate, we measure the escape probability. Equations (1) and (2) are obtained from the general time evolution by using the approximated operators $U_{\mathrm{h},i}$ describing the situations where the qubit is held resonant with either one of the TLSs. We then have

$$P_i(t) \approx |\langle 1|U_{\mathrm{iS}}U_{\mathrm{h},i}(t_{\mathrm{h}})U_{\mathrm{iS}}|g_1 1 g_2\rangle|^2, \quad i = 1, 2. \tag{5}$$

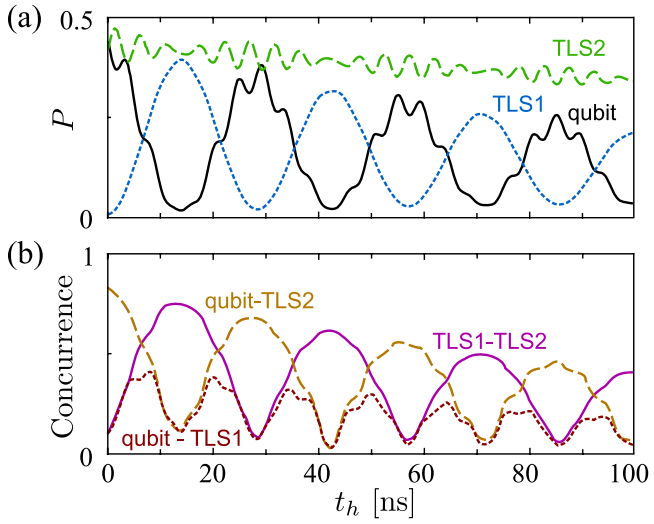

Figure 5. Simulation of the excitation probability of, and entanglement between, each of the three system components before the second $\sqrt{\text{iSWAP}}$. (a) Simulated excitation probabilities of the qubit (solid), TLS1 (dotted) and TLS2 (dashed), while holding the qubit at resonance with TLS1 for the time t_h. (b) The concurrence between each individual pair of subsystems (qubit–TLS2, dashed line; qubit–TLS1, dotted line; TLS1–TLS2, solid line) after tracing out the third component.

5. Three-way entanglement between the qubit and two-level states

However, for theoretical analysis of the tripartite dynamics the interesting state of the system is just before the final $\sqrt{\text{iSWAP}}$; as this is before TLS2 it is disentangled from the system. At the resonance frequency of TLS1 $\omega_\text{h} = \omega_1$, we find the approximated expression for the state vector to be

$$|\Psi_0(\omega_\text{h} = \omega_1, t_\text{h})\rangle \approx U_{\text{h},1}(t_\text{h}) U_{\text{iS}} |g_1 1 g_2\rangle$$
$$= -\frac{\text{i}}{\sqrt{2}} |g_1 0 e_2\rangle + \frac{\text{e}^{-\text{i}\Delta_{21} t_\text{h}}}{\sqrt{2}} \left(-\text{i} \sin \frac{v_1 t_\text{h}}{2} |e_1 0 g_2\rangle + \cos \frac{v_1 t_\text{h}}{2} |g_1 1 g_2\rangle \right). \quad (6)$$

As expected, half of the population is located in TLS2 and its state $|g_1 0 e_2\rangle$ does not show any coherent time evolution. In contrast, the qubit and TLS1 exchange population while accumulating a phase with respect to TLS2 with the frequency Δ_{21}. The population of the various components obtained from the numerical treatment is plotted in figure 5(a). Here, fast oscillations in the probability curves of the qubit and TLS2, which have opposite phase, can be recognized. They indicate that the qubit–TLS2 coupling is still not negligible but this does not disrupt the overall dynamics. The vanishing and reappearing of the fast oscillations indicate the presence of two frequencies that are close to each other. This is consistent with the spectrum of the oscillations shown in figures 3(b) and (d) and by equation (2), which yields the two frequencies $\Delta_{21} \pm v_1/2$.

To further study this interplay between the two defects, we use our theoretical model to calculate the entanglement present in the tripartite system. In figure 5(b), we plot the

concurrence [32] between each pair of system components (while tracing over the third). The concurrence is an entanglement measure yielding a number between 0 (no entanglement) and 1 (full entanglement). The initial entanglement between the qubit and TLS2 (via the $\sqrt{\text{iSWAP}}$) subsequently oscillates between the different components, reaching a maximum between TLS2 and either the qubit or TLS1, depending of the location of the majority of the population. In contrast, the concurrence between the qubit and TLS1 shows a beating with double frequency, as the maximal entanglement between these two subsystems is established twice a cycle. Interspersed between these points, we see points of genuine tripartite entanglement, due to the interaction between all three components. This multipartite entanglement is of the W state class, as our initial condition restricts us to the single-excitation subspace and therefore the 'three-tangle' is precisely zero [33, 34]. We note that tripartite entanglement of the W-type was recently reported for systems consisting of three superconducting qubits [35, 36].

6. Summary

In conclusion, we have presented evidence for controlled interaction between two microscopic defect states mediated by a phase qubit. During the implementation of the pulse sequence, the tunable qubit serves as a quantum shuttle, providing a bridge between two TLSs and establishing *a coherent tripartite interaction*. The Fourier spectrum of the observed qubit–TLSs beating contains clear evidence of such an interaction between all parts of the system over a time scale limited by the coherence of the system. This demonstration shows the possibility of using coherent interaction between many TLSs for the implementation of quantum gates.

Acknowledgments

We thank M Ansmann and J M Martinis (UCSB) for providing us with the sample that we measured in this work. This work was supported by the CFN of DFG, the EU projects SOLID and MIDAS and the US ARO under contract no. W911NF-09-1-0336.

References

[1] Nielsen M A and Chuang I L 2000 *Quantum Computation and Quantum Information* (Cambridge: Cambridge University Press)
[2] Roos C F, Riebe M, Häffner H, Hänsel W, Benhelm J, Lancaster G P T, Becher C, Schmidt-Kaler F and Blatt R 2004 *Science* **304** 1478
[3] Neumann P, Mizuochi N, Rempp F, Hemmer P, Watanabe H, Yamasaki S, Jacques V, Gaebel T, Jelezko F and Wrachtrup J 2001 *Science* **320** 1326
[4] Knill E, Laflamme R and Milburn G J 2001 *Nature* **409** 46
[5] Makhlin Y, Schön G and Shnirman A 2001 *Rev. Mod. Phys.* **73** 357
[6] Devoret M H, Wallraff A and Martinis J M 2004 arXiv:cond-mat/0411174
[7] Plastina F and Falci G 2003 *Phys. Rev.* B **67** 224514
[8] Silinpäa M A, Park J I and Simmonds R W 2007 *Nature* **449** 438
[9] Niskanen A O, Harrabi K, Yoshihara F, Nakamura Y, Lloyd S and Tsai J S 2007 *Science* **316** 723
[10] Fink J M, Bianchetti R, Baur M, Goeppl M, Steffen L, Filipp S, Leek P J, Blais A and Wallraff A 2009 *Phys. Rev. Lett.* **103** 083601
[11] Ansmann M *et al* 2009 *Nature* **461** 504

[12] Koch J, Yu T M, Gambetta J, Houck A A, Schuster D I, Majer J, Blais A, Devoret M H, Girvin S M and Schoelkopf R J 2007 *Phys. Rev.* A **76** 042319
[13] Manucharyan V E, Koch J, Glazman L I and Devoret M H 2009 *Science* **326** 113
[14] Phillips W A 1972 *J. Low Temp. Phys.* **7** 351
[15] Anderson P W, Halperin B I and Varma C M 1972 *Phil. Mag.* **25** 1478
[16] Zolfagharkhani G, Gaidarzhy A, Shim S, Badzey R L and Mohanty P 2005 *Phys. Rev.* B **72** 224101
[17] Macfarlane R M, Sun Y, Sellin P B and Cone R L 2006 *Phys. Rev. Lett.* **96** 033602
[18] Arcizet O, Rivière R, Schliesser A, Anetsberger G and Kippenberg T J 2009 *Phys. Rev.* A **80** 021803
[19] Venkatesan A, Lulla K J, Patton M J, Armour A D, Mellor C J and Owers-Bradley J R 2010 *J. Low Temp. Phys.* **158** 685
[20] Macha P, van der Ploeg S H W, Oelsner G, Il'ichev E, Meyer H-G, Wünsch S and Siegel M 2010 *Appl. Phys. Lett.* **96** 062503
[21] Hoehne F, Pashkin Yu A, Astafiev O, Faoro L, Ioffe L B, Nakamura Y and Tsai J S 2010 *Phys. Rev.* B **81** 184112
[22] Simmonds R W, Lang K M, Hite D A, Nam S, Pappas D P and Martinis J M 2004 *Phys. Rev. Lett.* **93** 7
[23] Martinis J M *et al* 2005 *Phys. Rev. Lett.* **95** 210503
[24] Palomaki T A, Dutta S K, Lewis R M, Przybysz A J, Paik H, Cooper B K, Kwon H, Anderson J R, Lobb C J and Wellstood F C 2010 *Phys. Rev.* B **81** 144503
[25] Neely M, Ansmann M, Bialczak R C, Hofheinz M, Katz N, Lucero E, O'Connell A, Wang H, Cleland A and Martinis J M 2008 *Nature Phys.* **4** 523
[26] Zagoskin A M, Ashhab S, Johansson J R and Nori F 2006 *Phys. Rev. Lett.* **97** 077001
[27] Lisenfeld J, Müller C, Cole J H, Bushev P, Lukashenko A, Shnirman A and Ustinov A V 2010 *Phys. Rev.* B **81** 100511
[28] Lisenfeld J, Müller C, Cole J H, Bushev P, Lukashenko A, Shnirman A and Ustinov A V 2010 *Phys. Rev. Lett.* **105** 230504
[29] Schuch N and Siewert J 2003 *Phys. Rev.* A **67** 032301
[30] Bushev P, Müller C, Cole J H, Lisenfeld J, Lukashenko A, Shnirman A and Ustinov A V 2010 *Phys. Rev.* B **82** 134530
[31] Lindblad G 1976 *Commun. Math. Phys.* **48** 119
[32] Wootters W K 1998 *Phys. Rev. Lett.* **80** 2245
[33] Coffman V, Kundu J and Wootters W K 2000 *Phys. Rev.* A **61** 052306
[34] Dür W, Vidal G and Cirac J I 2000 *Phys. Rev.* A **62** 062314
[35] Neeley M *et al* 2010 *Nature* **467** 570
[36] DiCarlo L, Reed M D, Sun L, Johnson B R, Chow J M, Gambetta J M, Frunzio L, Girvin S M, Devoret M H and Schoelkopf R J 2010 *Nature* **467** 574